Molecular dynamics reveals a novel Regulatory Ca^{2+}-Binding Site in the Mitochondrial Calcium Uniporter

Leandro Matías Sommese [1#*], Nicolás Palopoli [1], Maria Silvina Fornasari [1], Gustavo Parisi [1], Toni Gabaldón[2,3,4,5], Ana Julia Velez Rueda [1#*]

Author(s) Address Information

[1] *Structural Bioinformatics Group, Departamento de Ciencia y Tecnología, Universidad Nacional de Quilmes - Consejo Nacional de Investigaciones Científicas y Técnicas (CONICET), Buenos Aires, Argentina.*

[2] *Barcelona Supercomputing Centre (BSC-CNS). Plaça Eusebi Güell, 1-3. 08034 Barcelona, Spain.*

[3]*Institute for Research in Biomedicine (IRB Barcelona), The Barcelona Institute of Science and Technology, Baldiri Reixac, 10, 08028 Barcelona, Spain*

[4]*Catalan Institution for Research and Advanced Studies (ICREA), Barcelona, Spain*

[5]*CIBER de Enfermedades Infecciosas, Instituto de Salud Carlos III, Madrid, Spain*

[#] Both authors contributed equally to this work.

[*] Corresponding author(s): anajuliavelezrueda@gmail.com (Ana Julia Velez Rueda), sommeseleandro@gmail.com (Leandro Matías Sommese)

Running title: *Sommese LM et al / Characterization of a Novel Regulatory Ca^{2+}-Binding Site in the Mitochondrial Calcium Uniporter*

Abstract

The mitochondrial Ca^{2+} uniporter (MCU) plays essential roles in energy production, cytosolic Ca^{2+} signaling, and regulation of cell death. The activity of this channel complex is modulated by Mitochondrial Calcium Uptake 1 (MICU1) and Mitochondrial Calcium Uptake 2 (MICU2) proteins in response to Ca^{2+} levels. In cardiomyocytes, MICU1 inhibits the uniporter in resting cells while it activates it during contraction when bound to Ca^{2+}. Despite its importance, the structural mechanisms driving MICU1's open-close switch remain unclear.

In this study, we used structural modeling combined with molecular dynamics simulations to investigate MICU1's conformational dynamics under varying Ca^{2+} concentrations. Our analysis identified a previously uncharacterized pseudo-EF-hand motif (pEF-h) that acts as an early calcium sensor, initiating conformational transitions that prime canonical EF-hand sites for subsequent calcium binding. Calcium binding induces substantial structural changes in MICU1, including a decrease in isoelectric point, shifts in surface charge distribution, and significant reductions in cavity volume, length, and hydrophobicity. Notably, a 53.4% reduction in intermolecular distances between key domains was observed during the transition from the apo to the Ca^{2+}-bound state.

These findings uncover a previously overlooked hierarchical activation of MICU1's calcium-binding sites and provide new mechanistic insights into the regulation of MCU. This

enhanced understanding of mitochondrial calcium signaling paves new ways to potential novel therapeutic strategies targeting calcium dysregulation in metabolic, cardiovascular, and neurodegenerative diseases.

Highlights

- A novel calcium-binding site in human's MICU1, featuring a unique helix–loop–β-sheet structure, was identified and functionally characterized.
- This new Ca^{2+}-binding site in MICU1 that acts as an early sensor, triggering structural changes key to its regulatory function.
- Calcium binding motif distributions and phylogenetic constraints show possible functional divergence.

KEYWORDS: Calcium Uniporter; MICU1; EF-hand motif; Conformational Diversity; Structural Dynamics

Introduction

The mitochondrial uniporter is a Ca^{2+} channel complex (mtCU) with important roles in energy production, cytosolic Ca^{2+} signaling, and cell death [1]. In mammals, the uniporter complex comprises four core components: the pore-forming MCU, the gatekeepers MICU1 and MICU2, and an auxiliary subunit EMRE essential for Ca^{2+} transport [2]. Tight regulation of the uniporter by cytosolic Ca^{2+} levels is crucial for maintaining physiological homeostasis [3–5].

MCU homologs are distributed widely across all major branches of the eukaryotic tree of life. Sequenced metazoa, plants, and protozoa typically have homologs of both MCU and MICU1 or lack both proteins, with the exception of mammals in which MCU and MICU1 physically interact and are highly co-expressed [6]. Furthermore, previous studies have proposed that the co-occurrence of MCU and MICU1 may have been evolutionarily advantageous in eukaryotes [7,8]. MICU1 appears to enhance organismal fitness by contributing to the selectivity of the mitochondrial calcium uniporter, thereby preventing toxic manganese overload and associated oxidative stress, while also supporting efficient calcium-dependent ATP production in high-energy-demand tissues. In mammals, MICU1 is also physically associated and co-expressed with MICU2, whose activity and physical association with the pore depend on the presence of MICU1.

The activity of the entire channel is known to be regulated by Ca^{2+} concentration through the concerted action of MICU1 and MICU2. In addition, it has been demonstrated that cells lacking MICU1 or MICU2 lose the normal threshold for Ca^{2+} intake [9]. In resting cardiomyocytes, mitochondrial MICU1 is free of Ca^{2+} and thus binds and inhibits MCU. The

release of Ca^{2+} from the endoplasmic reticulum leads to an increase in cytosolic Ca^{2+} concentration. Upon cardiomyocyte contraction, MICU1 binds Ca^{2+} thereby activating the MCU channel, which triggers in massive Ca^{2+} uptake by mitochondria. The resulting decrease in cytosolic Ca^{2+} concentration below the activation threshold causes Ca^{2+} dissociation from MICU1, inhibiting the MCU channel [10].

MICU1 provides cooperative activation as cytosolic Ca^{2+} concentration rises above a certain threshold, thereby allowing mitochondria to properly decode different inputs [11]. Csordás and co-authors compared mitochondrial Ca^{2+} uptake differences between wild type and MICU1-deficient cells, and they demonstrated that its two functional Ca^{2+}-binding EF-hand motifs (EF-h) in the protein were important in the transition between fully closed and open states of MCU. Even though the authors suggested that MICU1 conformational changes may mediate the regulation of multiple specific functions required in different cell contexts, the structural mechanisms underlying this switch mechanism remain unknown. The mtCU's Ca^{2+}-dependent regulation hinges on dynamic interactions among MCU, MICU1, MICU2, and EMRE. In low Ca^{2+} (<1 μM), MICU1's conserved K/R ring (residues K126, R128, R129, R130, R132) binds MCU's acidic pore entrance (D261, E264), blocking ion flux, while its N-terminal polybasic domain (residues 99–110) and C-terminal helix (residues 440–443, including R440/R442) stabilize the MCU-MICU1 interface. MICU1 further anchors to EMRE via electrostatic interactions between its polybasic region and EMRE's acidic C-terminal tail (D68/E72). Both MICUs form a Ca^{2+}-sensing heterodimer through critical EF-h interactions (between MICU1 D231/D235 and MICU2 R352). When Ca^{2+} concentration rises, cooperative binding to the MICU1-MICU2 heterodimer induces a 30° rotation of MICU1's EF1 helix (α6), displacing pore-contacting residues (R259/R261/R263) and reorienting the K/R ring (K126/R129), thereby unblocking the pore. Throughout this gating cycle, EMRE maintains MICU1 proximity to MCU, ensuring rapid channel re-closure upon Ca^{2+} decrease [12].

MtCU has been associated with different diseases [13–15], highlighting its clinical relevance in human health. Particularly, MICU1 dysfunction leads to severe pathological conditions due to impaired calcium homeostasis in mitochondria [16]. In Parkinson's disease, MICU1 is crucial for neuronal survival by regulating calcium efflux from mitochondria via the Na^{+}/Ca^{2+} exchanger, where its dysfunction leads to mitochondrial calcium overload and increased vulnerability to cell death [13]. Studies in pancreatic β-cells have demonstrated that both MICU1 and MCU are essential for proper insulin secretion, as their knockdown significantly reduces glucose-stimulated insulin secretion by affecting mitochondrial Ca^{2+} uptake and ATP production [14]. Moreover, in diabetic cardiomyopathy, MICU1 deficiency in cardiac microvascular endothelial cells leads to excessive mitochondrial calcium uptake and homeostasis imbalance, causing nitrification stress-induced endothelial damage and inflammation that disrupts the myocardial microvascular endothelial barrier function [15].

Loss-of-function mutations in MICU1 result in a complex disease phenotype characterized by proximal muscle weakness, learning difficulties, and extrapyramidal motor disturbances [17,18]. To date, 13 pathogenic MICU1 variants have been identified, with mutations occurring through different mechanisms including splice site mutations, nonsense variants, missense variants, and deletions [17,19]. However, the structural basis underlying the functional effects of many of these mutations is still unclear. In particular, the precise conformational transitions that enable MICU1 to switch between inhibitory and permissive states in response to calcium remain incompletely characterized, especially in the context of its interaction with other components of the MCU complex [9,10]. Additionally, the contribution of non-canonical motifs—such as the recently identified pseudo-EF-hand—to MICU1's sensing and gating behavior has not been fully explored in vivo. Moreover, how tissue-specific expression and post-translational modifications modulate MICU1 activity across different physiological and pathological conditions is still largely unknown [11,20]. Addressing these gaps is essential to fully decipher MICU1's role in mitochondrial signaling and to develop targeted interventions for MICU1-related disorders.

In this study, we identify and characterize a previously unrecognized pseudo-EF-hand (pEF-h) motif in MICU1, that could be related with its gatekeeping regulation. Through computational modeling and molecular dynamics simulations, we detail the conformational changes induced by Ca^{2+} binding and uncover a stepwise activation mechanism. Our results indicate that the pEF-h acts as an early calcium sensor, triggering structural rearrangements that facilitate subsequent Ca^{2+} binding at the canonical EF-hand sites. These conformational shifts impact charge distribution, protein flexibility, and intramolecular interactions, ultimately modulating MICU1's gating function over mitochondrial calcium uptake. Furthermore, we observed a progressive decrease in Gibbs free energy (ΔG) upon calcium binding—first at the pEF-h, then at the canonical EF-h sites—suggesting an cooperative mechanism in which initial binding enhances overall calcium affinity. By identifying this novel regulatory element, our findings deepen the understanding of MICU1's structural dynamics and functional regulation, setting the stage for future studies on its role in mitochondrial calcium homeostasis and its involvement in conditions such as diabetic cardiomyopathy and neurodegenerative diseases.

Results

Calcium-Driven Conformational Dynamics of MICU1

The regulatory subunit MICU1 is a large protein, comprising 476 amino acids and weighting approximately 54 kDa. The region between residues 1 and 110 undergoes order-disorder transitions. This region constitutes a compositionally biased sequence subdomain, with basic

and acidic residues at the MCU-MICU1 interface [21]. Given that all MICU1 tridimensional structures available in Protein Data Bank (PDB) are incomplete [22], we performed the structural modeling of the 30% missing part of MICU1 using AlphaFold2 [23] (Total pDDLT > 70) followed by molecular dynamics minimization. In order to address persistent knowledge gaps regarding the conformational transitions that enable MICU1's regulatory function, we explored the conformational changes upon calcium binding. The structure inspection allowed us to discover a previously unknown Ca^{2+} binding site present in both the fully unbound and fully Ca^{2+}-bound forms, which is located within a region between the Ser138 and Glu200 that is absent in the available PDB structures. We characterized this region as a pseudo-EF-HAND motif (pEF-h), as its structural configuration deviates from the canonical EF-h motif [25] –the canonical linear motif DXDXNG(X)5E with ***α***-loop-***α*** structure– having instead linear motif EXE(X)3DEG(X)7E with ***α***-loop-***β*** structure (See Figure 1). Despite this structural divergence, the site I facilitates calcium coordination, and appears to play a crucial role in the protein's calcium handling and the structural and functional shifts driven by Ca^{2+} binding, as suggested by the results presented below.

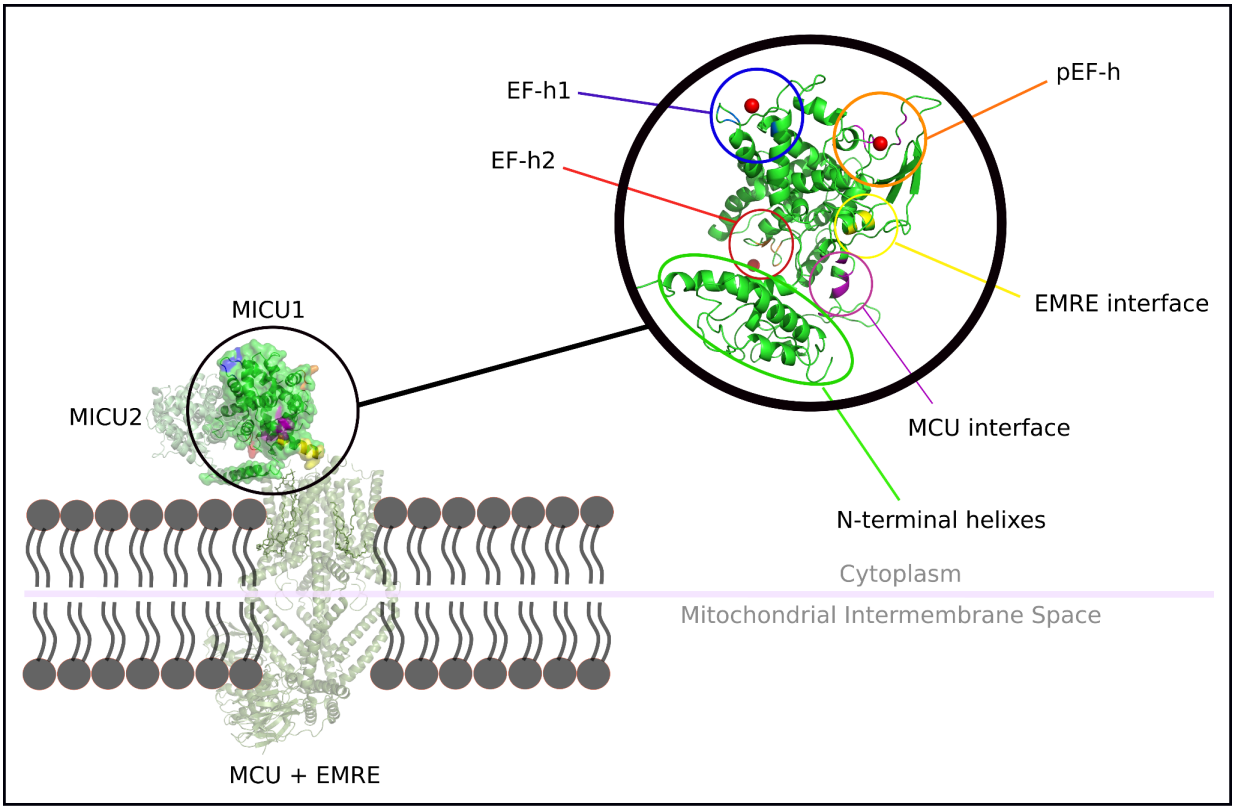

Fig. 1. Mitochondrial Ca^{2+} uniporter (MCU) components with MICU1 (green) calcium binding regions. The pseudo EF-hand motif is shown in orange, characterized by a linear EXE(X)$_3$DEG(X)$_7$E sequence and a typical α-loop-β structural arrangement. The green region represents the N-terminal alpha-helices that undergo order-disorder transitions upon calcium binding. Blue indicates the canonical EF-hand 1, while red marks EF-hand 2, located proximally to the MICU2 binding site. The purple region highlights the MCU interaction interface, and the yellow region denotes the EMRE interaction site.

For the purpose of exploring MICU1's calcium-dependent structural transitions, we analyzed its sequence composition and charge distribution with localCIDER [24]. The Janus analysis [25,26] —aimed to identify metamorphic proteins that exhibit fold-switching depending on environmental conditions– revealed a sequence with context-dependent conformational flexibility, expected to collapse or expand based on environmental conditions [26]. Given the hypothesis that MICU1 works as an on-off switch depending on Ca^{2+} concentration [27], we computationally simulated the titration of MICU1 by performing molecular dynamics in solvation solutions containing 0, 0.15, 0.05, and 0.01 M Ca^{2+}. We observed clear structural differences between the unbound and bound form. The interaction with Ca^{2+} at 0.15 M induced significant structural changes (RMSD = 13.17 Å), leading to a decrease in the isoelectric point from 10.03 to 2.93 and altering the protein's net charge from +1 to -1, under the same pH and ionic force conditions. Additionally, Ca^{2+} binding reduced the volume, length, and hydrophobicity of all MICU1's cavities by 14.28%, 27.5%, and 41.7%, respectively.

One of the most interesting observations was the order-disorder transition in the N-terminal region, guided by Ca^{2+} binding (Fig. 1). This negatively charged polyampholyte region forms three alpha helices capable of coordinating multiple Ca^{2+} ions through electrostatic interactions with non conserved negative residues in it. The distances between the EMRE-binding alkaline motif and the Ca^{2+} binding site II substantially decrease, for example the most drastic changes being observed are between residues K351 and D421, which decreases from 13.0 to 11.3 Å after binding to Ca^{2+}, and between residues K340 and E432 that go from 19.2 to 13.9 Å (Figure 1A). The calcium presence promotes the reorientation of residues K340 and K341, disrupting the interactions sustained with the MICU II/EMRE site through hydrogen bonding with residues D78 and E79, and E432. This movement ultimately exposes interaction region II, facilitating binding between these two proteins in a new orientation. This structural change triggered by calcium binding allows the exposure of its relevant binding sites to MCU and EMRE (Figure 2B).

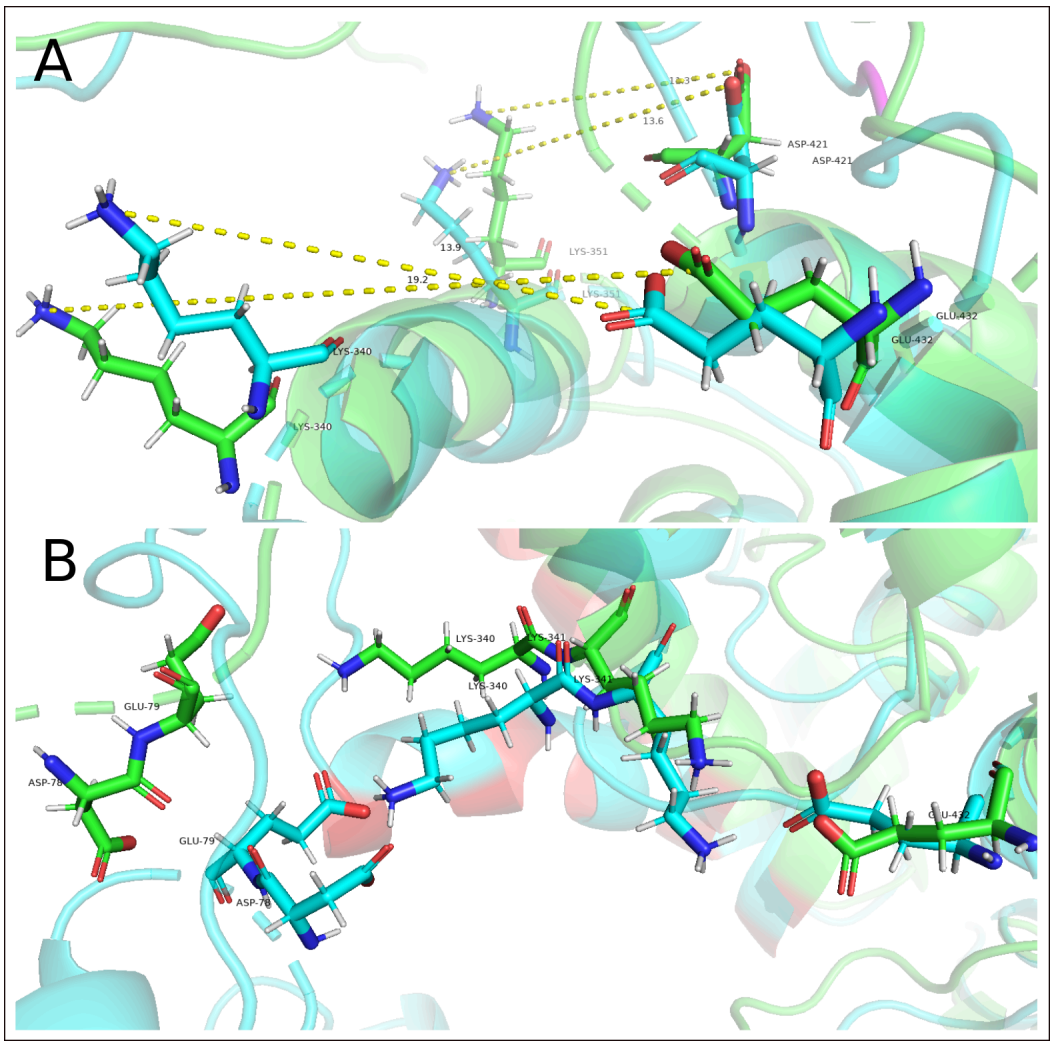

Fig. 2. Calcium binding (cyan) induces structural rearrangements that reduce distances between the EMRE-binding alkaline motif and Ca^{2+} site II, compared to the unbound state (green); 1A) Notable reductions occur between K351–D421 (13.0→11.3 Å) and K340–E432 (19.2→13.9 Å); 1B) This reorientation disrupts interactions with MICU1/EMRE (D78, E79, E432), exposing interaction region II and enabling new MCU-EMRE binding.

Interestingly, we observed an intermolecular distance reduction between EF-hand sites 1 and 2 showed a substantial reduction of 53.4% upon transition from unbound to fully Ca^{2+}-bound forms (See Table 1). Similarly, the pEF-h site also undergoes a significant reduction in intermolecular distance upon Ca^{2+} binding (from 11.3 Å to 6.6 Å), highlighting its role in calcium coordination (See Table 1). Notably, during the increase of calcium concentration (from 10mM to 150mM), the Ca^{2+} binding sites exhibit cross-activation between the unbound and fully Ca^{2+}-bound forms, along with a pKa shift (-0.55/0.33).

	EF-h1			EF-h2				pEF-h
	D231/ N233	N233/ D235	K290/ E242	D423/ E427	N425/ E432	D421/ E432	D421/ D423	S138/ E200
Unbound	7.2 A	5.9 A	7.1 A	12.9 A	11.6 A	5.9 A	5.9 A	11.3 A
Fully Ca^{2+}-bound	2.9 A	4.4 A	5.4 A	8.0 A	6.3 A	8.7 A	5.4 A	6.6 A

Table 1. Distances between residues within calcium-binding sites, indicating the spatial relationships during unbound and fully Ca^{2+}-bound states. The values are measured in angstroms (Å) and represent the proximity of specific residue pairs involved in calcium coordination.

Regulation of MICU1 Function and Energetics Through Calcium Binding

Furthermore, to understand the functional role of these three sites in the on-off switch transitions, we evaluated their stickiness and occupancy. For the first metric, we measured the duration each calcium ion remained bound to a site, while for the second, we assessed the proportion of residues at each site that maintained contact with calcium. Molecular dynamics analysis revealed that at high calcium concentrations ([Ca^{2+}] > 50mM), we observe the permanent occupation of pEF-h and EF-h1 during throughout the entire trajectory, and a late occupation of EF-hand2, preceding the protein disorder-order transition in N-terminal region (Figure 3). At lower calcium concentrations ([Ca^{2+}] = 10 mM), EF-h2 does not exhibit permanent calcium occupation, although both the pEF-h and EF-h1 sites establish contacts with the ion. Notably, even though the pEF-h site binds calcium earlier than EF-h1, the latter maintains more persistent contacts. This lack of complete binding at low calcium concentrations indicates that the protein cannot fully fold, as reflected in the reduced permanence and occupancy. In summary, we observed a temporal sequence in calcium binding: calcium first binds to the pEF-h site, which acts as a sensitive calcium sensor. This initial binding induces conformational changes that subsequently enable the EF-hand sites to bind calcium. These findings suggest that both pEF-h and EF-hand sites play a crucial role in the open-close switching mechanism of the channel (Fig. 3).

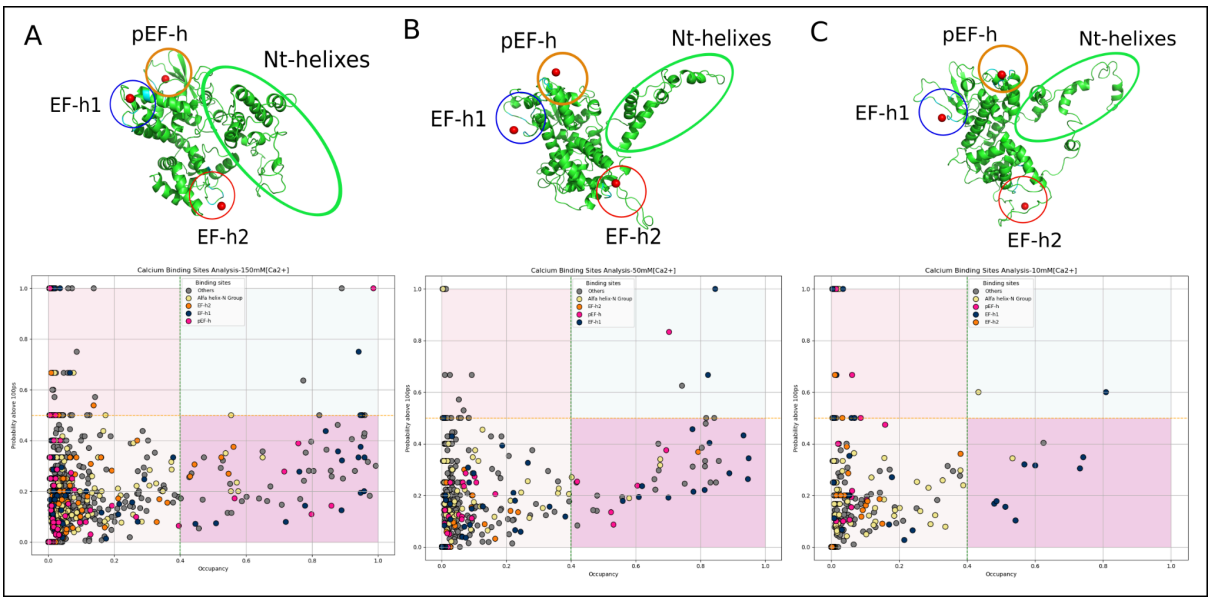

Fig. 3. Calcium-binding site analysis across different calcium concentrations (150 mM, 50 mM, and 10 mM). Each scatterplot shows the occupancy and maximum permanence time (in picoseconds) of protein residues interacting with Ca^{2+} ions, calculated from molecular dynamics simulations. The background is divided into colored regions defined by occupancy and permanence thresholds (vertical and horizontal lines, respectively), highlighting zones of high interaction strength. Residues are color-coded according to their structural group: EF-h1 site (dark blue), EF-h2 site (orange), pEF-h site (pink), and N-terminal α-region (khaki); non-functional or low-interaction sites are shown in gray. Each point represents a protein residue, with those located in the upper right quadrant—showing high occupancy and long permanence—corresponding to strong and persistent calcium-binding sites. Each panel reflects the interaction behavior under a distinct calcium concentration: 1A) 150 mM shows numerous residues with strong and persistent interactions, consistent with fully formed calcium-binding sites; 1B) 50 mM displays moderately reduced interaction strength, with fewer residues exhibiting high occupancy and permanence, suggesting partial engagement of binding sites; 1C) 10 mM reveals generally low occupancy and short permanence times, indicating the protein fails to achieve stable and complete folding under these conditions. For each case, a protein structure is shown, with the N-terminal helices highlighted in yellow, the EF-hands and pEF-hand in black, and calcium ions in red.

To better understand the relationship between the sites' roles and calcium concentration, we analyzed the total protein ΔG of interactions to metals using FoldX over all the conformers. Our analysis revealed that pEF-h binding to calcium decreases the ΔG of interactions with bound metals upon binding (in 6.20 kjoules/mol), favouring the occupancy of the rest of the calcium binding sites (EF-h1 and EF-h2) through the conformational changes induced by the metal binding. This decrease grows upon each EF-hand is occupied, suggesting a cooperative behavior between the calcium binding sites (Fig. 4). Furthermore, this decrease in protein's ΔG of interactions to metals accompanies an increased proportion in the exposure of negative charged residues: the percentage of negative charged residue in the protein' surface grow a 24.7%, 43.6 and 61.6% at 0.15, 0.05, and 0.01 M Ca^{2+} respectively.

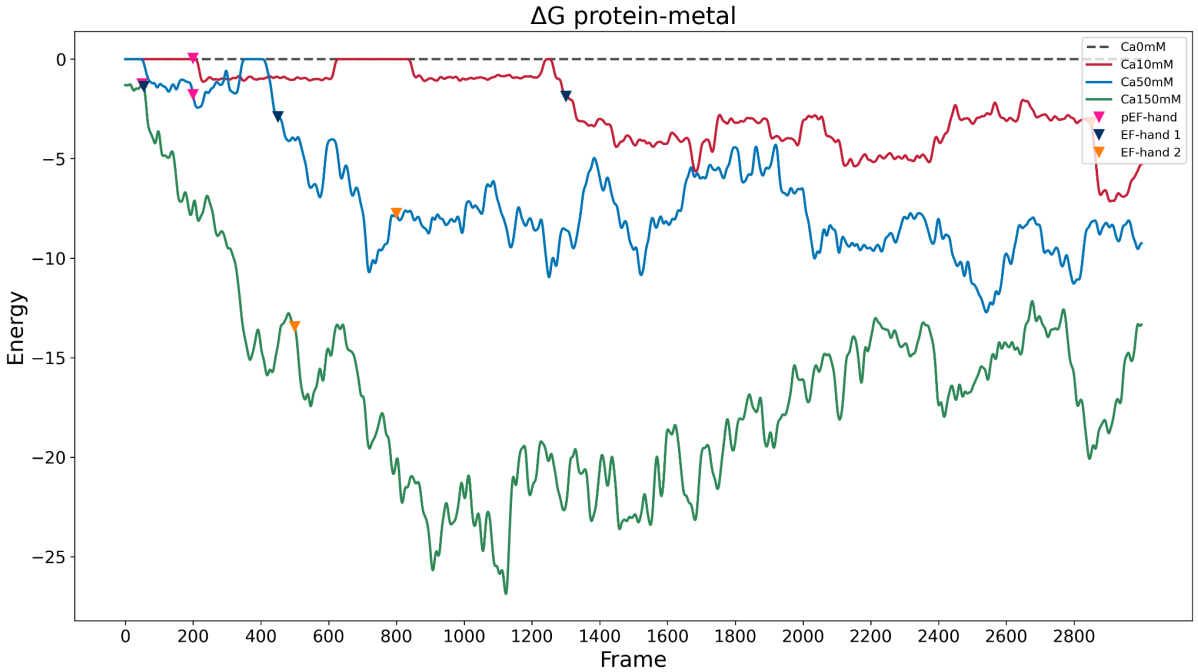

Fig. 4. ΔG of interactions to metals per frame: in green (150 mM), orange (50 mM), and blue (10 mM). Binding at pEF-h and EF-hand I and II sites reduces the ΔG of protein-metal after Ca^{2+} binding. Colorful arrows show the pEF-hand (pink), EF-hand1 (blue) and EF-hand2 (orange) saturation.

Evolutionary pEF-hand calcium-binding motif conservation

To better understand pEF-hand evolution and its relation with function, we examined the distribution of conserved calcium-binding motifs within the pEF-hand region and the presence or absence of the different mtCU members across species. To this aim, we retrieved 292 MICU1 orthologs from OMA database [29], and aligned them using Clustal [30,31]. We explored its evolutionary conservation through phylogenetic inference using IQ-TREE with maximum likelihood methods [28]. Among the 292 analyzed sequences, the DXNXDG$(X)_5$E motif was the most prevalent, present in 57.53% of cases, and likely associated with stable calcium coordination rather than rapid regulatory shifts (Fig. 5). The DXDXDG$(X)_5$E and EXE$(X)_3$DED$(X)_7$E motifs followed in frequency, found in 20.21% and 15.41% of sequences, respectively.

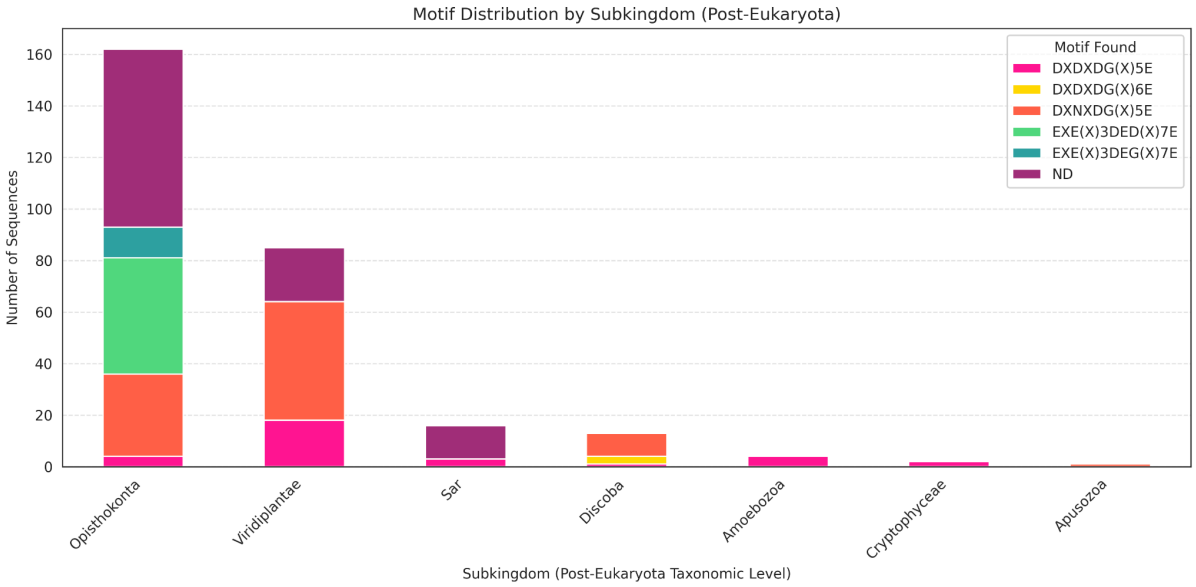

Fig. 5. Distribution of conserved pEF-hand calcium-binding motifs across major eukaryotic subkingdoms. Stacked bar plot showing the frequency of four conserved putative calcium-binding motifs—DXNXDG$(X)_5$E, DXDXDG$(X)_5$E, EXE$(X)_3$DED$(X)_7$E, and EXE$(X)_3$DEG$(X)_7$E—within the pEF-hand region across representative eukaryotic subkingdoms.

In contrast, the canonical EF-hand-like motif EXE$(X)_3$DEG$(X)_7$E was rare (3.77%) but notable for its presence in metazoans such as *Homo sapiens*. When mapped to phylogenetic groups, motif usage exhibited a strong lineage-specific pattern (Fig. 6). The non-canonical DXNXDG$(X)_5$E motif was especially dominant in Viridiplantae and Discoba, while Opisthokonts—encompassing animals and fungi—showed a broader motif distribution, including all four major types. Our analysis highlights the prevalence of the DXNXDG$(X)_5$E motif (57.53%), which correlates with stable calcium coordination in plants and Discoba. In contrast, the canonical EXE$(X)_3$DEG$(X)_7$E motif, though rare (3.77%), is exclusive to metazoans, where it underpins high-affinity binding (occupancy: 0.84 ± 0.04; permanency: 17.8 ± 4.1 ns) (Table 2).

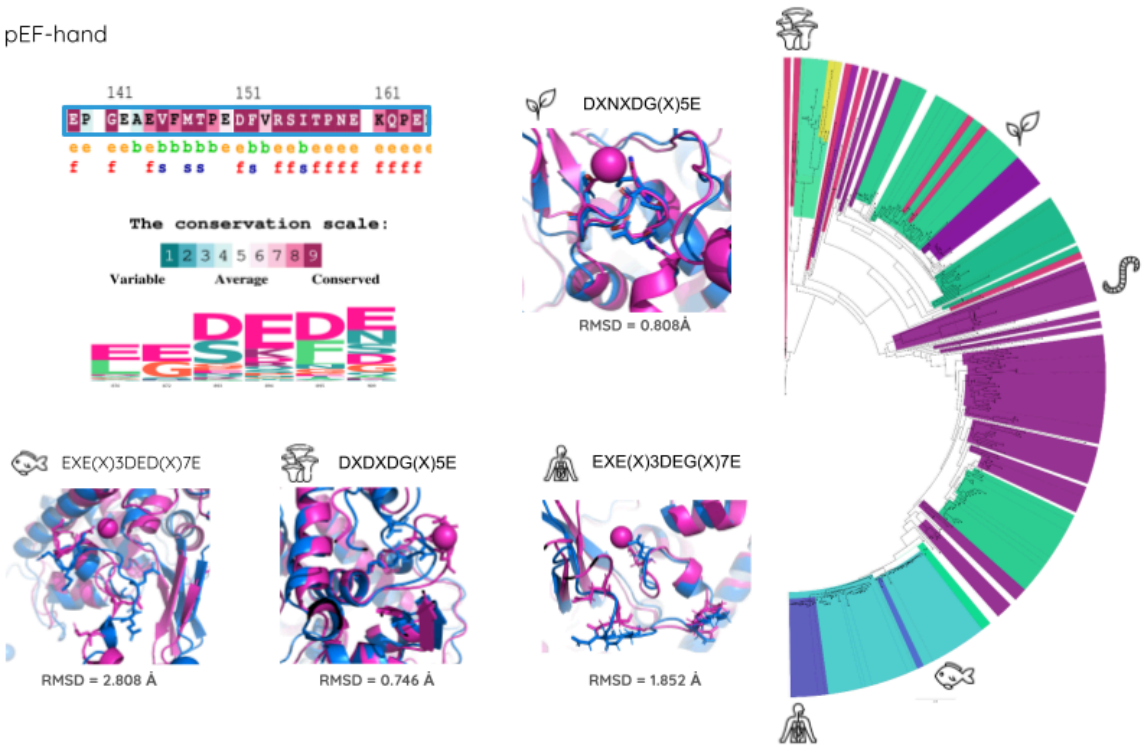

Fig. 6. Calcium-binding motifs—DXNXDG(X)$_5$E, DXDXDG(X)$_5$E, EXE(X)$_3$DED(X)$_7$E, EXE(X)$_3$DEG(X)$_7$E, DXDXE(X)4E— in Cluster's representatives pEF-hand sites. Pseudo EF-hand motifs mapped to the phylogenetic tree, showing lineage-specific patterns across eukaryotic evolution. In green we represent the sequences including the DXNXDG(X)$_5$E, in blue and light blue the EXE(X)$_3$DEG(X)$_7$E and the EXE(X)$_3$DED(X)$_7$E variants; in pink the DXNXDG(X)$_5$E variant, and in purple those without a motif in the region.

These findings position the pEF-hand as a versatile regulatory module, where structural conservation permits functional plasticity—from a dynamic sensor in basal eukaryotes to a high-fidelity calcium gatekeeper in vertebrates. Future studies could probe whether pEF-hand variations directly influence mitochondrial calcium dynamics in non-metazoan systems, where its role remains less defined.

Structural and Evolutionary Constraints Over Calcium Binding Sites

To investigate MICU1's binding sites variations and possible functional adaptations across the species, we first made a sequence clustering using CD-HIT [32], in order to identify representative proteins among the phylogenetic tree for a deep structural and functional comparison of their pEF-hand and EF-hand motifs.

For each cluster representative sequence, including human MICU1, we structurally characterized them through 10 ns molecular dynamics simulations (at 0.15 M Ca^{2+}), and calculated the metal-binding affinities using FoldX across all simulation frames. This integrative approach enabled comparative evaluation of calcium-binding affinity across MICU1 orthologs and provided insight into lineage-specific adaptations in EF-hand calcium

coordination.

The pEF-hand region (residues 138–200), essential for calcium coordination, exhibits significant evolutionary divergence across eukaryotes (Table 2). In Amoebozoa, this region retains a canonical EF-hand motif with the classical helix-loop-helix structure, whereas in mammals, despite broader structural divergence across Eukarya, the pEF-hand sequence remains highly conserved, underscoring its critical role in calcium regulation [33]. In contrast, plants such as *Macleaya cordata* maintain the overall structural architecture but display substantial sequence variation, resulting in the loss of the canonical EF-hand motif and reduced calcium-binding occupancy (0.14 ± 0.02) compared to metazoans. This suggests potential functional adaptations or alternative biological roles, as proposed for motif variants in other systems [34–36].

Taxa	mtCU	Motifs order	Site	Sequence Pattern Binding Ca+2	Structural Pattern	Total Occupancy/Max Permanency (ns)		Minimum Metal Binds energy Ca+2
Lepisosteus oculatus **(Animalia Chordata)**	MCU MICU1 MICU2 EMRE	poliK, pEF-h, EF-h1, EF-h2	pEF-h	EXE$(X)_3$DED$(X)_7$E	***α***-loop-***β***	0.60±0.06	4.5±0.9	-4.26
			EF-h1	DXNXDG$(X)_5$E	***α***-loop-***α***	0.65±0.08	4.5±1.1	-4.80
			EF-h2	DXDXNG$(X)_5$E	***α***-loop-***α***	0.52±0.06	3.3±0.4	-3.70
Macleaya cordata **(Plantae Magnoliopsida)**	MCU MICU1	(no poliK), pEF-h, EF-h1, EF-h2	EF-h3	DXNXDG$(X)_5$E	***α***-loop-***α***	0.67±0.09	3.6±1.0	-3.55
			EF-h1	DXDXNG$(X)_5$E	***α***-loop-***α***	0.46±0.005	2.4±0.5	-3.68
			EF-h2	DXNXDG$(X)_5$E	***α***-loop-***β***	0.14±0.02	1.0±0.1	-2.97
Angiostrongylus costaricensis **(Animalia Nematoda)**	MCU MICU1 EMRE	poliK, pEF-h EF-h1, EF-h2	pEF-h	DXDXE$(X)_4$E	***β***-loop-***β***	0.68±0.03	6.5±0.4	-7.16
			EF-h1	DXNXDG$(X)_5$E	***α***-loop-***α***	0.62±0.04	5.5±0.6	-4.89
			EF-h2	DXNXDG$(X)_5$E	***α***-loop-***α***	0.47±0.06	3.1±0.8	-3.51
Dictyostelium discoideum **(Protista Mycetozoa)**	MCU MICU1	(no poliK), pEF-h, EF-h1, EF-h2	pEF-h	DXDXDG$(X)_5$E	***α***-loop	0.86±0.04	5.2±1.5	-3.25
			EF-h1	DXNXDG$(X)_5$E	***α***-loop-***α***	0.38±0.04	1.3±0.2	-2.76
			EF-h2	DXDXNG$(X)_5$E	***α***-loop-***α***	0.52±0.07	3.1±0.9	-4.30
Homo Sapiens **(Animalia Chordata)**	MCU MICU1 MICU2 EMRE	poliK, pEF-h, EF-h1, EF-h2	pEF-h	EXE$(X)_3$DEG$(X)_7$E	***α***-loop-***β***	0.84±0.04	17.8±4.1	-6.20
			EF-h1	DXNXDG$(X)_5$E	***α***-loop-***α***	0.87±0.04	18.7±3.3	-4.62
			EF-h2	DXDXNG$(X)_5$E	***α***-loop-***α***	0.41±0.05	8.6±1.8	-5.49

Table 2. Calcium binding motifs in the pEF-h and MCU complex characteristics for sequence cluster's representatives. Cluster's representatives pEF-hand sites, including Humans, were characterized in their sequence pattern, occupancy and permanency and minimum metal binding energies. The minimum metal binding energies were measured over all the frames obtained in a 10ns molecular dynamics at 0.15M [Ca+2].

The DxDxDG motif, traditionally linked to EF-hand structures, is now recognized in diverse structural contexts, indicating evolutionary repurposing rather than a single ancestral origin [34,37]. The EF-hand function is mostly structural in bacteria and regulatory in eukaryotes [35,38]. Nevertheless, some exceptions to the trend were demonstrated in some eukaryotes, where the EF-hand occasionally displays a high affinity that leads to a purely structural role [39]. Our comparative analysis reveals striking lineage-specific differences in calcium-binding dynamics. The EF-hand domains exhibit further specialization across lineages. While human EF-h1 displays near-maximal occupancy (0.87 ± 0.04), prolonged Ca^{2+} permanency (18.7 ± 3.3 ns), and relatively low binding energy (−4.62 kcal/mol), the nematode *Angiostrongylus costaricensis*—despite retaining an EF-h3 motif—shows intermediate occupancy (0.47 ± 0.06), shorter permanency (3.1 ± 0.8 ns), and comparatively higher binding energy (−3.51 kcal/mol), possibly reflecting functional divergence. These variations suggest that while the EF-hand's structural scaffold is conserved, its functional output is fine-tuned to meet lineage-specific regulatory demands. Notably, the presence of EMRE in vertebrates coincides with both the retention of this motif and energetically favorable binding (e.g., human EF-h1: −4.62 kcal/mol), whereas its absence in *Macleaya* and *Dictyostelium* coincides with weaker interactions (e.g., Macleaya EF-h2: −2.97 kcal/mol). These observations support the hypothesis that EMRE co-evolved with specialized EF-hand motifs to enhance calcium sensitivity in complex multicellular organisms [36–38].

When analyzing the pEF-hand, we observe for example in vertebrates –such as Lepisosteus oculatus and humans– this domain adopts an α-loop-β conformation with high calcium occupancy (0.60–0.84), prolonged permanency (4.5–17.8 ns), and notably low binding energies (−4.26 to −6.20 kcal/mol), suggesting a role in stable calcium coordination. The lower binding energy in humans (−6.20 kcal/mol) could further indicate evolutionary optimization for high-affinity binding, likely critical for fine-tuned regulation of mitochondrial calcium uptake in complex tissues (Table 2). In plants (*Macleaya cordata*) and amoebozoans (*Dictyostelium discoideum*) demonstrates more dynamic behavior. While *Dictyostelium* achieves high occupancy (0.86 ± 0.04), its shorter Ca^{2+} permanency (5.2 ± 1.5 ns) and moderate binding energy (−3.25 kcal/mol), along with the absence of EMRE, suggest a role in rapid calcium sensing rather than long-term storage. Macleaya, despite retaining an α-loop-α structure, shows the weakest binding across all representatives (0.14 ± 0.02 occupancy, 1.0 ± 0.1 ns permanency, −2.97 kcal/mol), implying either a secondary role in calcium sensing or a divergent regulatory mechanism.

Conclusion

Our study provides new structural and evolutionary insights into the role of MICU1 in

regulating the mitochondrial calcium uniporter complex, deepening our understanding of its function in calcium signaling and energy homeostasis. Through structural modeling and molecular dynamics simulations, we characterized calcium-induced conformational changes in MICU1, revealing substantial shifts in global structure, charge distribution, and cavity architecture upon Ca^{2+} binding.

A central finding was the identification of a previously uncharacterized calcium-binding motif, the pEF-h, located between residues 138–200. Distinct from canonical EF-hand motifs, the pEF-h adopts a helix-loop–β-sheet configuration while retaining functional calcium-binding capability. Our simulations indicate that this motif acts as an early Ca^{2+} sensor, initiating structural transitions that facilitate subsequent binding at EF-hand I and II, thus playing a pivotal role in MICU1's on–off regulatory mechanism.

Our evolutionary analysis further underscores the functional relevance of the pEF-h region. Among 292 analyzed sequences, we found that non-canonical motifs predominate in lineages such as Viridiplantae and Discoba, while rare but canonical $EXE(X)_3DEG(X)_7E$ motifs are observed in lineages such as metazoans. These motif distributions suggest strong phylogenetic constraints and possible functional divergence. Notably, the emergence of EMRE seems to accompany the presence of specialized motifs and more energetically favorable calcium binding in organisms such as Homo sapiens and Lepisosteus oculatus, implying a co-evolution of structural features for tighter Ca^{2+} control. Conversely, the absence of EMRE in taxa like *Dictyostelium discoideum* and *Macleaya cordata* is associated with weaker or absent calcium binding in the pEF-h region, possibly reflecting functional degeneration or reduced regulatory precision.

By integrating sequence conservation, structural modeling, dynamic simulations, and motif evolution, our study offers a comprehensive view of MICU1's calcium-dependent conformational landscape. These findings not only clarify the molecular basis of MICU1-mediated MCU regulation but may also inform future therapeutic approaches targeting mitochondrial Ca^{2+} uptake in metabolic, cardiovascular, and neurodegenerative diseases.

Materials and Methods

Structure Modelling and Molecular Dynamics

To investigate the conformational dynamics of MICU1, we performed structural modeling using AlphaFold2 [23], based on the incomplete three-dimensional structure available in the Protein Data Bank (PDB ID: 4NSC). The model was generated using default AlphaFold2 parameters.

Molecular dynamics simulations were carried out using GROMACS [40], to explore MICU1's structural changes at varying Ca^{2+} concentrations (0, 10, 50, and 150 mM). The

concentrations chosen assume that the close proximity between MICU and the Ryanodine Receptor, generates a high Ca^{2+}-microenvironment [41,42], and thus the concentrations needed for observing the conformational changes sustaining the protein function will be higher than the cytosolic one.

Each simulation was run for 30 nanoseconds using an all-atom representation with the CHARMM36 force field and TIP3P water model [43]. The starting conformation for the fully unbound form was taken from the structure at 0 mM Ca^{2+}, while the fully Ca^{2+}-bound form was defined as the structure with occupied EF-h sites.

Structural Analysis

Janus analysis was performed following the methodology described by Madhurima et al [26]. The structural characterization of MICU1 in the bond and unbound cavities forms were performed using CaviDB [44] to analyze cavity properties, including volume, hydrophobicity, and solvent accessibility. Key structural parameters, such as root mean square deviation (RMSD), accessible surface area (ASA), and residue-residue contacts, were calculated to assess conformational changes upon Ca^{2+} binding.

For comparative analysis, unbound and fully Ca^{2+}-bound conformations were structurally aligned using Chimera [45], enabling the quantification of residue distance changes.

The occupancies and permanency of calcium ions within the MICU1 pEF-hand and EF-hand motifs were computed from molecular dynamics simulations conducted. The total occupancy was defined as the fraction of simulation time in which a calcium ion remained coordinated within the canonical EF-hand motif binding site, averaged across replicates. Permanency was calculated as the maximum continuous time (in nanoseconds) that a calcium ion remained bound during the trajectory.

The metal binding energy was calculated using FoldX [46] by applying the MetalScan command across all frames of the trajectory. FoldX estimates the binding energy of calcium ions to protein motifs based on a semi-empirical energy function that includes van der Waals interactions, solvation, and metal coordination terms. The minimum binding energy (kcal/mol) was reported as the lowest energy value observed across the entire simulation.

All structural and dynamic data were processed using custom Python scripts, incorporating the MDAnalysis, Seaborn, Pandas, and SciPy libraries [47–49].

Evolutionary Analysis

To investigate the evolutionary conservation of MICU1, we performed phylogenetic inference using IQ-TREE with maximum likelihood methods [28]. A total number of 292 sequences were extracted from the OMA database [29] and aligned using Clustal [30] before sequence clustering with CD-HIT [32] –using 90% identity and a window equal 4 as parameters– which

grouped sequences by identity to track the sequential and structural conservation of the pEF-h motif.

The metal binding energy for the pEF-h and EF-hand sites in the homologs was measured using FoldX's metal binding command [46], over all the trajectory from Ca+2-free to fully bound. We took the minimum metal binding energy as reference for the interspecies comparison of the calculated energies.

The motifs' sequence patterns distribution were analyzed using custom Python scripts, incorporating the Seaborn, Pandas, and Numpy libraries [47–49].

Authors' contributions

LMS and AJVR carried out the bioinformatic analysis. TG carried out the evolutionary analysis conceptualization. NP carried out the linear motifs analysis conceptualization. AJVR and LMS conceived of the study, and participated in its design and coordination. GP and MSF carried out the project administration and funding acquisition. All authors participated in drafting the manuscript, as well as the final manuscript reading and approval.

Competing interests

The authors have declared no competing interests.

Acknowledgements

This work was supported by the National Council of Science and Technology of Argentina (CONICET).

References

[1] T.E. Gunter, D.R. Pfeiffer, Mechanisms by which mitochondria transport calcium., Am. J. Physiol. 258 (1990) C755-86. https://doi.org/10.1152/ajpcell.1990.258.5.C755.

[2] C. Wang, A. Jacewicz, B.D. Delgado, R. Baradaran, S.B. Long, Structures reveal gatekeeping of the mitochondrial Ca2+ uniporter by MICU1-MICU2., ELife. 9 (2020). https://doi.org/10.7554/eLife.59991.

[3] D. De Stefani, R. Rizzuto, T. Pozzan, Enjoy the trip: calcium in mitochondria back and forth., Annu. Rev. Biochem. 85 (2016) 161–192. https://doi.org/10.1146/annurev-biochem-060614-034216.

[4] C. Giorgi, S. Marchi, P. Pinton, The machineries, regulation and cellular functions of mitochondrial calcium., Nat. Rev. Mol. Cell Biol. 19 (2018) 713–730. https://doi.org/10.1038/s41580-018-0052-8.

[5] R. Rizzuto, D. De Stefani, A. Raffaello, C. Mammucari, Mitochondria as sensors and regulators of calcium signalling., Nat. Rev. Mol. Cell Biol. 13 (2012) 566–578. https://doi.org/10.1038/nrm3412.

[6] A.G. Bick, S.E. Calvo, V.K. Mootha, Evolutionary diversity of the mitochondrial calcium uniporter., Science. 336 (2012) 886. https://doi.org/10.1126/science.1214977.

[7] J. Wettmarshausen, V. Goh, K.-T. Huang, D.M. Arduino, U. Tripathi, A. Leimpek, Y. Cheng, A.A. Pittis, T. Gabaldón, D. Mokranjac, G. Hajnóczky, F. Perocchi, MICU1 Confers Protection from MCU-Dependent Manganese Toxicity., Cell Rep. 25 (2018) 1425-1435.e7. https://doi.org/10.1016/j.celrep.2018.10.037.

[8] D. Vecellio Reane, F. Vallese, V. Checchetto, L. Acquasaliente, G. Butera, V. De Filippis, I. Szabò, G. Zanotti, R. Rizzuto, A. Raffaello, A MICU1 splice variant confers high sensitivity to the mitochondrial ca2+ uptake machinery of skeletal muscle., Mol. Cell. 64 (2016) 760–773. https://doi.org/10.1016/j.molcel.2016.10.001.

[9] K.J. Kamer, V.K. Mootha, MICU1 and MICU2 play nonredundant roles in the regulation of the mitochondrial calcium uniporter., EMBO Rep. 15 (2014) 299–307. https://doi.org/10.1002/embr.201337946.

[10] M. Patron, V. Checchetto, A. Raffaello, E. Teardo, D. Vecellio Reane, M. Mantoan, V. Granatiero, I. Szabò, D. De Stefani, R. Rizzuto, MICU1 and MICU2 finely tune the mitochondrial Ca2+ uniporter by exerting opposite effects on MCU activity., Mol. Cell. 53 (2014) 726–737. https://doi.org/10.1016/j.molcel.2014.01.013.

[11] G. Csordás, T. Golenár, E.L. Seifert, K.J. Kamer, Y. Sancak, F. Perocchi, C. Moffat, D. Weaver, S. de la F. Perez, R. Bogorad, V. Koteliansky, J. Adijanto, V.K. Mootha, G. Hajnóczky, MICU1 controls both the threshold and cooperative activation of the mitochondrial Ca^{2+} uniporter., Cell Metab. 17 (2013) 976–987. https://doi.org/10.1016/j.cmet.2013.04.020.

[12] J.F. Garbincius, J.W. Elrod, Mitochondrial calcium exchange in physiology and disease., Physiol. Rev. 102 (2022) 893–992. https://doi.org/10.1152/physrev.00041.2020.

[13] S. Gandhi, A. Wood-Kaczmar, Z. Yao, H. Plun-Favreau, E. Deas, K. Klupsch, J. Downward, D.S. Latchman, S.J. Tabrizi, N.W. Wood, M.R. Duchen, A.Y. Abramov, PINK1-associated Parkinson's disease is caused by neuronal vulnerability to calcium-induced cell death., Mol. Cell. 33 (2009) 627–638. https://doi.org/10.1016/j.molcel.2009.02.013.

[14] M.R. Alam, L.N. Groschner, W. Parichatikanond, L. Kuo, A.I. Bondarenko, R. Rost, M. Waldeck-Weiermair, R. Malli, W.F. Graier, Mitochondrial Ca2+ uptake 1 (MICU1) and mitochondrial ca2+ uniporter (MCU) contribute to metabolism-secretion coupling in clonal pancreatic β-cells., J. Biol. Chem. 287 (2012) 34445–34454.

https://doi.org/10.1074/jbc.M112.392084.

[15] X. Shi, C. Liu, J. Chen, S. Zhou, Y. Li, X. Zhao, J. Xing, J. Xue, F. Liu, F. Li, Endothelial MICU1 alleviates diabetic cardiomyopathy by attenuating nitrative stress-mediated cardiac microvascular injury., Cardiovasc. Diabetol. 22 (2023) 216. https://doi.org/10.1186/s12933-023-01941-1.

[16] G. Bhosale, J.A. Sharpe, A. Koh, A. Kouli, G. Szabadkai, M.R. Duchen, Pathological consequences of MICU1 mutations on mitochondrial calcium signalling and bioenergetics., Biochim. Biophys. Acta Mol. Cell Res. 1864 (2017) 1009–1017. https://doi.org/10.1016/j.bbamcr.2017.01.015.

[17] F. Bitarafan, M. Khodaeian, E. Amjadi Sardehaei, F.Z. Darvishi, N. Almadani, Y. Nilipour, M. Garshasbi, Identification of a novel MICU1 nonsense variant causes myopathy with extrapyramidal signs in an Iranian consanguineous family., Mol. Cell. Pediatr. 8 (2021) 6. https://doi.org/10.1186/s40348-021-00116-w.

[18] C.V. Logan, G. Szabadkai, J.A. Sharpe, D.A. Parry, S. Torelli, A.-M. Childs, M. Kriek, R. Phadke, C.A. Johnson, N.Y. Roberts, D.T. Bonthron, K.A. Pysden, T. Whyte, I. Munteanu, A.R. Foley, G. Wheway, K. Szymanska, S. Natarajan, Z.A. Abdelhamed, J.E. Morgan, E. Sheridan, Loss-of-function mutations in MICU1 cause a brain and muscle disorder linked to primary alterations in mitochondrial calcium signaling., Nat. Genet. 46 (2014) 188–193. https://doi.org/10.1038/ng.2851.

[19] D. Lewis-Smith, K.J. Kamer, H. Griffin, A.-M. Childs, K. Pysden, D. Titov, J. Duff, A. Pyle, R.W. Taylor, P. Yu-Wai-Man, V. Ramesh, R. Horvath, V.K. Mootha, P.F. Chinnery, Homozygous deletion in MICU1 presenting with fatigue and lethargy in childhood., Neurol. Genet. 2 (2016) e59. https://doi.org/10.1212/NXG.0000000000000059.

[20] J.C. Liu, J. Liu, K.M. Holmström, S. Menazza, R.J. Parks, M.M. Fergusson, Z.-X. Yu, D.A. Springer, C. Halsey, C. Liu, E. Murphy, T. Finkel, MICU1 serves as a molecular gatekeeper to prevent in vivo mitochondrial calcium overload., Cell Rep. 16 (2016) 1561–1573. https://doi.org/10.1016/j.celrep.2016.07.011.

[21] N.E. Hoffman, H.C. Chandramoorthy, S. Shamugapriya, X. Zhang, S. Rajan, K. Mallilankaraman, R.K. Gandhirajan, R.J. Vagnozzi, L.M. Ferrer, K. Sreekrishnanilayam, K. Natarajaseenivasan, S. Vallem, T. Force, E.T. Choi, J.Y. Cheung, M. Madesh, MICU1 motifs define mitochondrial calcium uniporter binding and activity., Cell Rep. 5 (2013) 1576–1588. https://doi.org/10.1016/j.celrep.2013.11.026.

[22] H.M. Berman, J. Westbrook, Z. Feng, G. Gilliland, T.N. Bhat, H. Weissig, I.N. Shindyalov, P.E. Bourne, The protein data bank., Nucleic Acids Res. 28 (2000) 235–242. https://doi.org/10.1093/nar/28.1.235.

[23] J. Jumper, R. Evans, A. Pritzel, T. Green, M. Figurnov, O. Ronneberger, K. Tunyasuvunakool, R. Bates, A. Žídek, A. Potapenko, A. Bridgland, C. Meyer, S.A.A.

Kohl, A.J. Ballard, A. Cowie, B. Romera-Paredes, S. Nikolov, R. Jain, J. Adler, T. Back, D. Hassabis, Highly accurate protein structure prediction with AlphaFold., Nature. 596 (2021) 583–589. https://doi.org/10.1038/s41586-021-03819-2.

[24] A.S. Holehouse, R.K. Das, J.N. Ahad, M.O.G. Richardson, R.V. Pappu, CIDER: Resources to Analyze Sequence-Ensemble Relationships of Intrinsically Disordered Proteins., Biophys. J. 112 (2017) 16–21. https://doi.org/10.1016/j.bpj.2016.11.3200.

[25] A. Pastore, P.A. Temussi, The two faces of Janus: functional interactions and protein aggregation., Curr. Opin. Struct. Biol. 22 (2012) 30–37. https://doi.org/10.1016/j.sbi.2011.11.007.

[26] K. Madhurima, B. Nandi, A. Sekhar, Metamorphic proteins: the Janus proteins of structural biology., Open Biol. 11 (2021) 210012. https://doi.org/10.1098/rsob.210012.

[27] W. Wu, Q. Shen, R. Zhang, Z. Qiu, Y. Wang, J. Zheng, Z. Jia, The structure of the MICU1-MICU2 complex unveils the regulation of the mitochondrial calcium uniporter., EMBO J. 39 (2020) e104285. https://doi.org/10.15252/embj.2019104285.

[28] B.Q. Minh, H.A. Schmidt, O. Chernomor, D. Schrempf, M.D. Woodhams, A. von Haeseler, R. Lanfear, IQ-TREE 2: New models and efficient methods for phylogenetic inference in the genomic era, Mol. Biol. Evol. 37 (2020) 1530–1534. https://doi.org/10.1093/molbev/msaa015.

[29] A.M. Altenhoff, N.M. Glover, C.-M. Train, K. Kaleb, A. Warwick Vesztrocy, D. Dylus, T.M. de Farias, K. Zile, C. Stevenson, J. Long, H. Redestig, G.H. Gonnet, C. Dessimoz, The OMA orthology database in 2018: retrieving evolutionary relationships among all domains of life through richer web and programmatic interfaces., Nucleic Acids Res. 46 (2018) D477–D485. https://doi.org/10.1093/nar/gkx1019.

[30] M.A. Larkin, G. Blackshields, N.P. Brown, R. Chenna, P.A. McGettigan, H. McWilliam, F. Valentin, I.M. Wallace, A. Wilm, R. Lopez, J.D. Thompson, T.J. Gibson, D.G. Higgins, Clustal W and Clustal X version 2.0., Bioinformatics. 23 (2007) 2947–2948. https://doi.org/10.1093/bioinformatics/btm404.

[31] F. Sievers, D.G. Higgins, Clustal Omega for making accurate alignments of many protein sequences., Protein Sci. 27 (2018) 135–145. https://doi.org/10.1002/pro.3290.

[32] Y. Huang, B. Niu, Y. Gao, L. Fu, W. Li, CD-HIT Suite: a web server for clustering and comparing biological sequences., Bioinformatics. 26 (2010) 680–682. https://doi.org/10.1093/bioinformatics/btq003.

[33] M.R. Nelson, W.J. Chazin, Structures of EF-hand Ca(2+)-binding proteins: diversity in the organization, packing and response to Ca2+ binding., Biometals. 11 (1998) 297–318.

[34] D.J. Rigden, M.Y. Galperin, The DxDxDG motif for calcium binding: multiple structural contexts and implications for evolution., J. Mol. Biol. 343 (2004) 971–984.

https://doi.org/10.1016/j.jmb.2004.08.077.

[35] D.J. Rigden, M.J. Jedrzejas, O.V. Moroz, M.Y. Galperin, Structural diversity of calcium-binding proteins in bacteria: single-handed EF-hands?, Trends Microbiol. 11 (2003) 295–297. https://doi.org/10.1016/s0966-842x(03)00153-7.

[36] K. Denessiouk, S. Permyakov, A. Denesyuk, E. Permyakov, M.S. Johnson, Two structural motifs within canonical EF-hand calcium-binding domains identify five different classes of calcium buffers and sensors., PLoS ONE. 9 (2014) e109287. https://doi.org/10.1371/journal.pone.0109287.

[37] E.A. Newcombe, C.B. Fernandes, J.E. Lundsgaard, I. Brakti, K. Lindorff-Larsen, A.E. Langkilde, K. Skriver, B.B. Kragelund, Insight into Calcium-Binding Motifs of Intrinsically Disordered Proteins., Biomolecules. 11 (2021). https://doi.org/10.3390/biom11081173.

[38] J. Michiels, C. Xi, J. Verhaert, J. Vanderleyden, The functions of Ca(2+) in bacteria: a role for EF-hand proteins?, Trends Microbiol. 10 (2002) 87–93. https://doi.org/10.1016/s0966-842x(01)02284-3.

[39] J.D. Potter, J. Gergely, The calcium and magnesium binding sites on troponin and their role in the regulation of myofibrillar adenosine triphosphatase., J. Biol. Chem. 250 (1975) 4628–4633.

[40] M.J. Abraham, T. Murtola, R. Schulz, S. Páll, J.C. Smith, B. Hess, E. Lindahl, GROMACS: High performance molecular simulations through multi-level parallelism from laptops to supercomputers, SoftwareX. 1–2 (2015) 19–25. https://doi.org/10.1016/j.softx.2015.06.001.

[41] H. Qi, L. Li, J. Shuai, Optimal microdomain crosstalk between endoplasmic reticulum and mitochondria for Ca2+ oscillations., Sci. Rep. 5 (2015) 7984. https://doi.org/10.1038/srep07984.

[42] S. De La Fuente, C. Fernandez-Sanz, C. Vail, E.J. Agra, K. Holmstrom, J. Sun, J. Mishra, D. Williams, T. Finkel, E. Murphy, S.K. Joseph, S.-S. Sheu, G. Csordás, Strategic positioning and biased activity of the mitochondrial calcium uniporter in cardiac muscle., J. Biol. Chem. 291 (2016) 23343–23362. https://doi.org/10.1074/jbc.M116.755496.

[43] J. Huang, S. Rauscher, G. Nawrocki, T. Ran, M. Feig, B.L. de Groot, H. Grubmüller, A.D. MacKerell, CHARMM36m: an improved force field for folded and intrinsically disordered proteins., Nat. Methods. 14 (2017) 71–73. https://doi.org/10.1038/nmeth.4067.

[44] A.J. Velez Rueda, F.L. Bulgarelli, N. Palopoli, G. Parisi, CaviDB: a database of cavities and their features in the structural and conformational space of proteins., Database (Oxford). 2023 (2023). https://doi.org/10.1093/database/baad010.

[45] E.F. Pettersen, T.D. Goddard, C.C. Huang, G.S. Couch, D.M. Greenblatt, E.C. Meng, T.E. Ferrin, UCSF Chimera—a visualization system for exploratory research and analysis., J. Comput. Chem. 25 (2004) 1605–1612. https://doi.org/10.1002/jcc.20084.

[46] J. Schymkowitz, J. Borg, F. Stricher, R. Nys, F. Rousseau, L. Serrano, The FoldX web server: an online force field., Nucleic Acids Res. 33 (2005) W382-8. https://doi.org/10.1093/nar/gki387.

[47] N. Michaud-Agrawal, E.J. Denning, T.B. Woolf, O. Beckstein, MDAnalysis: a toolkit for the analysis of molecular dynamics simulations., J. Comput. Chem. 32 (2011) 2319–2327. https://doi.org/10.1002/jcc.21787.

[48] P. Virtanen, R. Gommers, T.E. Oliphant, M. Haberland, T. Reddy, D. Cournapeau, E. Burovski, P. Peterson, W. Weckesser, J. Bright, S.J. van der Walt, M. Brett, J. Wilson, K.J. Millman, N. Mayorov, A.R.J. Nelson, E. Jones, R. Kern, E. Larson, C.J. Carey, SciPy 1.0 Contributors, SciPy 1.0: fundamental algorithms for scientific computing in Python., Nat. Methods. 17 (2020) 261–272. https://doi.org/10.1038/s41592-019-0686-2.

[49] M. Waskom, seaborn: statistical data visualization, JOSS. 6 (2021) 3021. https://doi.org/10.21105/joss.03021.